Journal of
Synchrotron Radiation

ISSN 0909-0495

Received 12 June 2006
Accepted 21 November 2006

Cryoradiolytic reduction of crystalline heme proteins: analysis by UV-Vis spectroscopy and X-ray crystallography

Thorsten Beitlich,[a] Karin Kühnel,[a] Clemens Schulze-Briese,[b] Robert L. Shoeman[a] and Ilme Schlichting[a]*

[a]Max Planck Institute for Medical Research, Department of Biomolecular Mechanisms, Jahnstrasse 29, 69120 Heidelberg, Germany, and [b]Swiss Light Source, Paul Scherrer Institute, CH-5232 Villigen-PSI, Switzerland. E-mail: ilme.schlichting@mpimf-heidelberg.mpg.de

The X-ray crystallographic analysis of redox-active systems may be complicated by photoreduction. Although radiolytic reduction by the probing X-ray beam may be exploited to generate otherwise short-lived reaction intermediates of metalloproteins, it is generally an undesired feature. Here, the X-ray-induced reduction of the three heme proteins myoglobin, cytochrome P450cam and chloroperoxidase has been followed by on-line UV-Vis absorption spectroscopy. All three systems showed a very rapid reduction of the heme iron. In chloroperoxidase the change of the ionization state from ferric to ferrous heme is associated with a movement of the heme-coordinating water molecule. The influence of the energy of the incident X-ray photons and of the presence of scavengers on the apparent reduction rate of ferric myoglobin crystals was analyzed.

Keywords: radiolytic reduction; photoreduction; myoglobin; cytochrome P450; chloroperoxidase; microspectrophotometer; energy dependence; hydrated electrons; radical scavengers; radiation damage.

© 2007 International Union of Crystallography
Printed in Singapore – all rights reserved

1. Introduction

Shortly after the determination of the first protein structure, it was realised that radiation damage can limit the usable amount of X-ray diffraction data of crystalline biological samples (Blake & Phillips, 1962). The situation has escalated with the use of radiation produced by third-generation synchrotron sources that produce orders-of-magnitude higher X-ray intensities than home sources. Cryo-cooling of the sample slows the diffusion of the free radicals created by the ionizing effects of X-rays, preserving the quality of the (crystalline) sample and increasing the amount of data that can be collected. Therefore, crystals are usually kept at cryogenic temperature, typically 100 K, for data collection, an approach dubbed cryocrystallography. However, even at cryogenic temperatures, radiation damage does not stop (reviewed by Garman & Owen, 2006). Similar to room-temperature experiments, the most noticeable effect is loss of resolution and, in fact, this is the phenomenon generally associated with radiation damage. Other effects are more difficult to spot, and require analysis of the diffraction data. These include non-specific effects like non-isomorphism, increase in Wilson *B*-factors, $R_{\rm sym}$ and mosaicity, as well as specific effects like breakage of disulfide bonds, decarboxylations and changes in covalent modifications, *e.g.* loss of heavy-atom derivatization (Weik *et al.*, 2000; Burmeister, 2000; Ravelli & McSweeney, 2000).

At X-ray energies typically used in macromolecular crystallography, the major cause of radiation damage is the photoelectric effect, which accounts for more than 80% of the interactions between X-rays and sample at 12 keV [the remaining interactions are shared roughly equally between inelastic (Compton) and elastic (Rayleigh) scattering] (Murray *et al.*, 2005). The absorption of an X-ray photon results in the ejection of a photoelectron. This leaves a hole in an inner shell which is filled up by an outer-shell electron under emission of a fluorescence photon or an Auger electron. The partitioning of these two processes depends on the binding energy of the electron. In biologically relevant light elements, the predominant relaxation process (99%) is through Auger electron emission. As this ionization event requires approximately 40 eV, an average X-ray photon of 13 keV can yield roughly 300 electrons when depositing its energy in the sample (Mozumder & Magee, 1966; Nave, 1995).

The generation of X-ray-induced electrons during diffraction data acquisition may be of particular impact for studies on redox-sensitive systems such as flavoproteins (Fedorov *et al.*, 2003; Kort *et al.*, 2004; Mees *et al.*, 2004) or metalloproteins (Schlichting *et al.*, 2000; Berglund *et al.*, 2002; Adam *et al.*, 2004; Wuerges *et al.*, 2004). Flavin and metal cofactors can

absorb free electrons thereby changing their oxidation states, which can affect their conformation and coordination, respectively, and thereby the three-dimensional structures of the ligating proteins. On the other hand, radiolytic reduction of metalloproteins is not only a nuisance; it can also be exploited to generate and trap otherwise unstable reaction intermediates (Schlichting *et al.*, 2000). Indeed, the field of radiation chemistry has a longstanding history of success in studying chemical and biological reaction intermediates (Klapper & Faraggi, 1979). A distinct advantage of combining low-temperature techniques with radiation chemistry is the ability to utilize selective annealing to trap sequential intermediates in an enzymatic process. The species can be investigated and characterized by a wide variety of methods: spectroscopic (ultraviolet, visible, infrared, Raman, CD, MCD, EPR, ENDOR and Mossbauer) as well as structural (X-ray diffraction and solid-state NMR). Cryoradiolytic approaches have seen a recent renaissance in mechanistic studies on heme enzymes (see, for example, Davydov, Macdonald *et al.*, 1999; Davydov, Yoshida *et al.*, 1999; Davydov *et al.*, 2001, 2002; Denisov *et al.*, 2002*a*,*b*, 2007).

Independent of whether the goal is to minimize the effects of cryoreduction or to exploit them productively, it is desirable to have an on-line monitoring system to identify the species being characterized crystallographically because X-rays serve not only as a probe but are in fact also a pump. For many metallo- and particularly hemoproteins this is relatively straightforward because they have unique UV-Vis absorption spectra (Eaton & Hofrichter, 1981) that are sensitive towards changes of the heme group and its surroundings. Their spectra can be monitored in crystals by microspectrophotometry as shown in a variety of publications (Hadfield & Hajdu, 1993; Bourgeois *et al.*, 2002; Murray & Garman, 2002; Sakai *et al.*, 2002; Berglund *et al.*, 2002; Wilmot *et al.*, 2002; Sato *et al.*, 2004, Weik *et al.*, 2002; Crosson & Moffat, 2002; Fedorov *et al.*, 2003; Pearson *et al.*, 2004).

The structural characterization of defined redox states is not a trivial task because electrons liberated in the sample by X-rays during crystallographic data collection can alter the redox state of the active site. Attempts to minimize radiation-induced structural changes in crystals include soaking them in excess electron scavengers, using short-wavelength X-rays or composite data-collection strategies. So far, no systematic study has been undertaken that probes the dependence of the rate of cryolytic reduction on the energy of the X-ray photons, or on the chemical composition of the mother liquor. We attempted this by studying three different hemoproteins: the oxygen storage protein myoglobin (Mb), a bacterial cytochrome P450, P450cam, and the related enzyme chloroperoxidase (CPO)[1]. Using on-line microspectroscopy we followed the changes in optical absorption spectra of crystals upon X-ray irradiation at beamline X10SA of the Swiss Light Source (SLS, Paul Scherrer Institute, Villigen, Switzerland) (Pohl *et al.*, 2006). We analyzed how fast the initial state decays, new intermediates are formed, and how stable they are. We also used this information productively to collect a data set of the low-spin ferric species of CPO.

2. Material and methods

2.1. Crystallization

All chemicals used were of analytical grade. Horse heart myoglobin (Sigma, catalogue number M1882) was crystallized at 293 K by equilibrating 10 µl drops obtained by the mixing of 5 µl protein (10 mg ml^{-1}) and 5 µl reservoir solution (3.4 *M* ammonium sulfate and 0.1 *M* Tris, HCl pH 8.0) against 1 ml reservoir solution using the hanging-drop geometry. Rosette-shaped clusters of thin crystal plates grew within a few days. Single-crystal plates (space group $P2_1$, a = 63.9 Å, b = 28.8 Å, c = 35.6 Å, β = 106.8°, one molecule of molecular weight 17 kD per asymmetric unit, solvent fraction 0.33, typical size 200 µm × 100 µm × 4 µm) of roughly equal thickness (4 µm) were separated from a rosette and transferred into a cryoprotectant solution containing 21.5% glycerol and 2.8 *M* ammonium sulfate. After a 30 s soak, the crystals were flash-cooled in liquid nitrogen.

Cytochrome P450cam was expressed, purified and crystallized as described (Schlichting *et al.*, 1997). Monoclinic crystals ($P2_1$, a = 67.8 Å, b = 62.8 Å, c = 95.5 Å, β = 90.6°, one molecule of molecular weight 45 kD per asymmetric unit, solvent fraction 0.47, typical size 150 µm × 80 µm × 50 µm) were used to generate the ferrous dioxygen-bound complex at 277 K (Schlichting *et al.*, 2000). Briefly, crystals were reduced chemically by a 10–20 min soak in a nitrogen-saturated solution containing 50 m*M* Tris HCl, pH 7.4, 250 m*M* KCl, 27% PEG 8000, and 100 m*M* sodium dithionite. After a brief washing step in a dithionate free solution supplemented with 20% glycerol, the crystals were placed into a home-made pressure cell and exposed to 50–100 bar of oxygen for 120 to 300 s. After slowly releasing the pressure, the crystals were flash-cooled in liquid nitrogen.

CPO from *Caldariomyces fumago* was expressed and purified as described (Blanke *et al.*, 1989). Crystals were grown by the hanging-drop method at 293 K. The reservoir solution contained 50 m*M* KBr, 20% PEG 3000, 0.1 *M* sodium citrate, pH 3.4; 1 µl of 15 mg ml^{-1} CPO in 5 m*M* sodium acetate buffer pH 3.8 was mixed with 1 µl of the reservoir solution. Rod-like orthorhombic crystals ($C222_1$, a = 57.7 Å, b = 150.5 Å, c = 100.8 Å, one molecule of molecular weight 42 kD per asymmetric unit, solvent fraction 0.52) grew within a few days. For cryoprotection, CPO crystals (average size ∼400 µm × 80 µm × 20 µm) were transferred in two steps (each taking 30 s to 1 min) into the cryoprotectant, first into a solution containing 5% sucrose, 5% xylitol, 50 m*M* KBr, 20% PEG 3000, 0.1 *M* sodium citrate, pH 3.4, and afterwards into the cryoprotectant consisting of 10% sucrose, 10% xylitol, 50 m*M* KBr, 20% PEG 3000, 0.1 *M* sodium citrate, pH 3.4, and then flash-cooled in liquid nitrogen.

[1] Mb and P450cam contain no disulfide bridges, whereas CPO has a single disulfide bond.

2.2. Single-crystal microspectrophotometry

UV-Vis absorption spectra of crystals kept at 100 K in a gaseous nitrogen stream (cryojet, Oxford Instruments) were measured with an XSPECTRA microspectrophotometer (4DX-ray Systems AB, Uppsala, Sweden) linked to an Oriel 77400 Multispec spectrometer, an Andor InstaSpec II photodiode array, and a Zeiss MCS 500 xenon light source. The microspectrophotometer was mounted at the diffractometer of beamline X10SA at the SLS (Villigen, Switzerland) to allow for simultaneous acquisition of optical spectra and of diffraction data. The microspectrophotometer focus had a diameter of 60 μm and was therefore smaller than both the crystal surface and the X-ray beam diameter ensuring that only the parts of the crystal were probed that were exposed to X-rays. Optical spectra were recorded before and during X-ray exposure and compared with reference spectra (both of crystals and solutions) to identify the species present. For the cryoradiolytic measurements, the crystals were oriented to measure absorption spectra while maintaining a large projection towards the X-ray beam. The incident X-ray energy ranged from 7 to 15 keV, with the photon flux adjusted to 10^9 to 10^{11} photons s^{-1} using appropriate absorbers. Photon fluxes were obtained from the photocurrent measured by a Si PIN diode (Syntef, Norway) on the beamline, assuming a linear relationship between photocurrent and flux at a given energy. In all experiments the beam was defocused [100 μm (full width at half-maximum Gaussian profile) × 100 μm (linear illumination) (h × v) for the myoglobin and chloroperoxidase experiments, and 100 μm × 120 μm for the studies on P450 (full width at half-maximum Gaussian profile in both dimensions)]. The storage-ring current was 300 mA throughout the experiments owing to top-up operation of the ring. During X-ray irradiation, optical absorption spectra were recorded with a temporal resolution of 0.02–0.05 s depending on saturation effects of the diode array. For P450, the spectra were taken with a repetition rate of 5 Hz. Spectra were evaluated with the Andor iDus program supplied with the photodiode array. First, the initial spectrum was subtracted from the kinetic series, yielding a series of difference spectra. Then absorbances at 555 nm were subtracted from the values at 566 nm in order to eliminate any uncorrelated underlying absorbance changes originating for example from solvated electrons (see §3.2.1). These time-dependent intensity changes were fitted using *GraFit* (Erithacus Software Limited, Surrey, UK) to a double-exponential equation with offset $y = A\exp(-k_1t) + B\exp(-k_2t) + C$, using simple weighting, as this was the simplest model to give no systematically varying residuals. From this fit the rate constants k_1 and k_2 were obtained with k_1 being defined as the faster one.

2.3. Dose calculation

To correlate the formation of intermediates with the amount of energy applied to the crystal, the absorbed dose D (Gy = J kg^{-1}) was calculated according to

$$D = \sigma eEnt/m,$$

where σ is the fractional beam absorption by the crystal, a function of beam and crystal properties, which can be obtained from the program *RADDOSE* (Murray *et al.*, 2004). The remaining constants are E, the X-ray photon energy (eV); e, the unit conversion factor ($e = 1.6 \times 10^{-19}$ J eV^{-1}); n, the photon flux (s^{-1}); t, the exposure time (s); and m, the mass of the irradiated crystal volume (kg). As we were not able to reliably measure the thickness of the myoglobin plates, we selected roughly equally sized crystals for our studies. They all had a thickness of around 4 μm and their surface area was in all cases larger than the X-ray beam size. As the beam did not change size between subsequent measurements of myoglobin crystals, the mass of irradiated crystal volume remains constant. Furthermore, sample thickness is not an issue at least for thin crystals, since both absorbed energy and mass are linearly dependent on the thickness, *i.e.* the dose is to first-order thickness independent. Since the absorption in the drop becomes important at low energies, care was taken to minimize the thickness of the cryoprotectant film in which the crystal was suspended. To examine possible correlations of photon energy concentration with the rate of radiolytic reduction of a protein crystal, it is necessary to normalize to the dose rate. For convenience, normalization in our case was performed with σ, E and n only, as m stayed the same for all crystals of the same heme protein. In the case of sodium ascorbate, sodium nitrate and nicotinamide, σ, E and n are constant, so no normalization was needed. In the case of the glycerol measurements, E and n are constant, so only the values of 0 and 40% glycerol content had to be normalized for σ due to the different concentration of ammonium sulfate in the cryoprotectant solution.

2.4. X-ray data collection and structure determination

Diffraction data from CPO crystals were collected at beamline X10SA (SLS, Switzerland) at 90 K. A composite data-collection scheme was employed to obtain 'low dose' and 'high dose' data sets (Berglund *et al.*, 2002; Fedorov *et al.*, 2003; Carugo & Carugo, 2005). The X-ray beam (12.7 keV) was defocused to 100 μm × 100 μm and a 100 μm Al absorber was inserted, yielding a flux of 1.2×10^{12} photons s^{-1}. Diffraction data were collected from 11 crystals using exposure times of 1 s per degree. After indexing using a single image, the crystals were orientated so as to maximize the unique data obtained from the first 10° of crystal rotation to yield a composite data set consisting of 10° wedges. After collection of the 'low dose' data slice, each crystal was exposed to X-rays for 1 min without an absorber (flux 1.7×10^{12} photons s^{-1}), and then the data collection was repeated with the 100 μm Al absorber in place. Data were processed and scaled using the *XDS* software package (Kabsch, 1993). The structure was determined by molecular replacement with *AMoRe* (Navaza, 2001) using the CPO structure (1cpo) (Sundaramoorthy *et al.*, 1995) as a search model. Refinement was carried out using *Refmac5* (Murshudov *et al.*, 1999) and model building was carried out using *COOT* (Emsley & Cowtan, 2004).

3. Results and discussion

Radiation damage has been recognized as a potentially limiting factor in X-ray crystallographic studies. Fortunately, however, in most cases the direct effects on the protein structure, such as decarboxylations of aspartate or glutamate side chains, can be identified readily since the expected results are well known from independent biochemical data that include the primary sequence and the occurrence of disulfide bonds. A special case of radiation damage is the photoreduction of redox-active groups such as of metals in metalloproteins. Although this phenomenon is well known from studies using extended X-ray absorption fine structure (EXAFS), X-ray absorption near-edge structure (XANES) and electron paramagnetic resonance (EPR) spectroscopy (see, for example, Chance *et al.*, 1980; Ericson *et al.*, 1988; Penner-Hahn *et al.*, 1989; Champloy *et al.*, 2000; Yano *et al.*, 2005), the diagnosis is difficult using only crystallographic data. Photoreduction-induced changes are often suspected only if there are discrepancies between the structural data and the information obtained from spectroscopic analysis (*e.g.* UV-Vis, Raman, EXAFS, XAS). Unfortunately, for many metalloproteins this independent information is not available, so one can even not decide *post mortem* whether the structure should be relabelled in terms of the presumed oxidation state. It is therefore important to use independent analytical tools, such as on-line microspectroscopy, to follow data collection and to identify parameters that slow cryoradiolytic reduction by the X-ray beam. We analyzed the cryoradiolytic reduction of three different crystalline heme proteins by on-line UV-Vis absorption microspectroscopy. The first objective was to find out how much of a problem, in terms of unintended reduction, the exposure to a defocused undulator beam at the SLS, a third-generation synchrotron, actually represents. The second objective was to test the influence of the X-ray energy and the addition of scavengers on the apparent reduction rate of the heme iron.

The time evolution of the absorbance changes occurring upon exposure of the crystals to X-rays was fitted by a double exponential function with offset, as described in §2. In all cases the faster process accounts for only $\sim$10% of the signal amplitude, and its rate constant (k_1) was an order of magnitude larger than the second one (k_2.) After an initial burst, the reduction is described by k_2 only. Therefore, we assume that this apparent rate constant describes the reduction after the concentration of solvated electrons inside the observed volume has reached a steady state. The apparent rate constant k_2 should be influenced by the number of solvated electrons, as well as the effectiveness of the scavenger molecules to capture electrons and to prevent them from reacting with the iron ion. On the other hand, k_1 should be influenced by the time the electrons take to reach this steady state, as well as by the concentration of electrons present during the equilibration process. We are aware that even though this equation fits the data, it might not be the one representing the real process. The rate of reduction depends on the concentration of electrons, which itself is a function of time, due to effects such as generation, recombination with radicals and scavengers, and photobleaching. Theoretical considerations have been made by Moan & Kaalhus (1973), but their model included too many variables to consistently fit our data.

Reduction rates for a given condition scattered by $\pm$15%, and corresponding data of multiple data sets were averaged to yield one data point, as displayed in the figures. In general, experiments on the effect of scavengers on the heme reduction rates should be repeated using more concentrations and for other heme proteins to gain statistical significance and to analyze the influence of the reduction potential of the heme iron.

3.1. Myoglobin

Myoglobin is a small heme-containing oxygen storage protein that has become a model system to study the structural dynamics of ligand binding. The three-dimensional structure of myoglobin was the first protein structure to be determined by X-ray crystallography and, in fact, the damaging effects of X-ray irradiation were first described for this system (Blake & Phillips, 1962). Cryoradiolytic reduction of the so-called met myoglobin [metMb: ferric (Fe^{3+}) myoglobin that has a water molecule bound at the sixth ligand position of the heme iron] results in the formation of a non-equilibrium ferrous (Fe^{2+}) state. Its temperature-induced relaxation has been followed spectroscopically (Prusakov *et al.*, 1995; Lamb *et al.*, 1998). However, in these studies no information was given on the dose required for reduction. A recent study using γ-radiolysis systematically analysed the protein concentration and dose dependence of cryoreduction yield (Denisov *et al.*, 2007). The study was undertaken because maximizing the yield of unstable redox intermediates generated in cryoradiolytic reduction experiments is crucial for the success of structural and spectroscopic studies on metalloenzyme mechanisms. Maximizing dose-dependent yield is not of immediate concern in studies using synchrotron radiation since the dose used in ^{60}Co γ-irradiation studies is orders of magnitude less than in crystallographic studies. In the latter case, however, the influence of the energy of the X-ray photons is an important variable that has not yet been investigated systematically.

Fig. 1 shows the changes in the UV-Vis absorption spectrum of metMb upon 10 keV X-ray irradiation. The first spectrum (Fig. 1*a*) corresponds to the non-irradiated crystalline metMb. Irradiation immediately results in the formation of new peaks. The Soret band shifts from 413 nm to 427 nm, two new double peaks at 528/536 and 556/566 nm arise, while the bands between 500 and 700 nm slowly decrease (see also Fig. 1*b*). These features, the red-shifted Soret band and the split *Q*-bands, agree well with reports on cryoreduced metMb (*e.g.* Lamb *et al.*, 1998; Denisov *et al.*, 2007). The effect of different doses on the spectra is compared in Fig. 1(*b*). Even before the dose limit of 30 MGy (Owen *et al.*, 2006) is reached, the whole spectrum decays slowly and loses its features. This is due to more and more damage occurring within the protein. Fig. 1(*c*) shows the time course of the absorption changes at 566 nm compared with the initial absorption values of the non-irra-

diated crystal. A maximum can be observed at a dose of around 2 MGy. Interestingly, this dose is much higher than the one reported recently (∼0.16 MGy) for a cryoradiolysis study performed at 77 K on frozen myoglobin solutions using ^{60}Co γ-irradiation (Denisov *et al.*, 2007). Several factors may contribute to this difference. (i) The chemical composition of the samples: higher glycerol concentrations (65%) are used in the aqueous glycerol glass sample (see §3.1.2), whereas the crystalline sample contains high concentrations of ammonium sulfate (2.7 *M*) and the protein concentration in the crystal is more than tenfold higher than in the most concentrated solution sample. Thus, amide radicals at the protein backbone (Jones *et al.*, 1987) can reach high concentrations and recombine by tunnelling of trapped electrons (Willard, 1973) and thereby shield the iron centres. Another reason could be the difference in mobility of water radicals, mostly hydroxyl radicals, and thus in the efficiency of recombination of radiolytic electrons with these radicals. Significant yields of trapped electrons have been found in organic glasses but not in similar crystalline systems. (ii) The different energy of the irradiation photons: 1.33 MeV for the ^{60}Co source, resulting in a large contribution of Compton scattering, *versus* ∼10 keV for the synchrotron source. (iii) Difference in obtaining the dose: it is calculated in the case of the X-ray study (Murray *et al.*, 2004), taking into account the protein, heme, ammonium sulfate and water. In the case of the ^{60}Co γ-irradiation experiment, the dose is measured using a calibrated Radiachromic film FWT-60-00 (Far West Technology, CA, USA). Its composition resembles that of an average protein (63.5% C, 12.0% N, 9.5% H, 14.8% O), but does not account for the heme iron, sulfur and phosphor (from the buffer). It seems, therefore, possible that the dose might be underestimated.

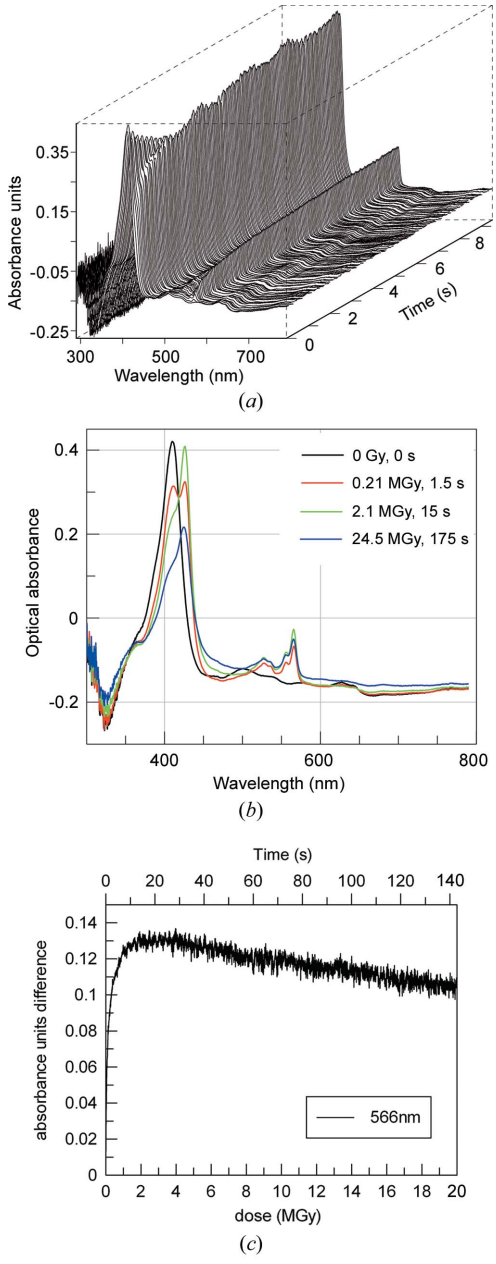

Figure 1
Cryoradiolytic reduction of met myoglobin crystals kept at 100 K. (*a*) Time course of the UV-Vis absorption spectrum of met myoglobin crystals during X-ray irradiation at 10 keV with a flux of 1.1 × 10^{12} photons s^{-1} and a focused beam. The temporal resolution is 50 ms. (*b*) Myoglobin absorption spectra taken before and after certain time-points after starting the X-ray irradiation. A new species forms rapidly (dose 0.2 MGy, red) after initiation of X-ray irradiation. This species reaches saturation after 15 s (dose 2 MGy, green). When approaching the dose limit (30 MGy; Owen *et al.*, 2006) the whole spectrum decays slowly (blue). (*c*) Time course of the 566 nm peak.

3.1.1. Energy dependence of photoreduction. Knowledge of the energy dependence of photoreduction is important for the design of diffraction data-collection schemes that either aim to minimize or to maximize cryoradiolytic reduction of the sample. However, so far no systematic study has been undertaken, and few data are available (Schlichting *et al.*, 2000; Berglund *et al.*, 2002). Therefore, we measured the rate of photoreduction of metMb for different energies of the X-ray beam. The apparent rate constants k_1 and k_2 of the reduction were normalized to the dose rate applied to the crystal, taking into account the dependence of the dose on the incident X-ray energy. As neither the focus size of the microspectrophotometer nor the crystal thickness changed during our measurements, normalization is only necessary for the energy of the beam as well as the flux and the absorption probability of the crystal at a given X-ray energy. Fig. 2 shows the results of measurements at energies of 7.0, 7.13, 9.0, 12.0 and 15.0 keV. A complex energy dependence of the normalized reduction rate is observed. Interestingly, both k_1 and k_2 increase from 7.0 keV to reach a maximum at 9.0 keV and decrease again at higher energies. This similar behaviour might have some yet unknown origin. Interestingly, the increase of the cross section of the photoeffect at 7.13 keV due to the iron absorption edge does not significantly influence the rates of radiolytic reduction. This is in line with the dose calculation that predicts an increase of the order of 10%. Moreover, the density of trapped electrons in the observed volume is high enough for the ferric iron ions to immediately capture an electron and convert to the Fe^{2+} species. The yield of trapped electrons in aqueous glycerol glasses at temperatures of 90–100 K is 1.5 per 100 eV (Makarov *et al.*, 1969). For a photon energy of 10 keV, a flux of 5.7 × 10^{11} photons s^{-1} and an absorption probability of 0.0024 thus yields 2.1 ×

10^{11} electrons s^{-1} for the volume of 1.2×10^{-14} m^3 (given by the diameter of the microspectrophotometer focus of 60 µm and a crystal thickness of 4 µm) which corresponds to 34 m*M* s^{-1}. The same volume contains 3.84×10^{11} protein molecules (corresponding to a concentration of 53 m*M*), so within seconds the protein concentration inside the sample becomes low compared with the concentration of trapped electrons. The lack of an increase of the radiolytic rate upon irradiating ferric metMb at the Fe-absorption edge is in agreement with the findings of an unrelated study that measured the energy dependence of the oxidation yield of ferrous ion in a Fricke solution irradiated with 1.8–10 keV X-rays (Watanabe *et al.*, 1995).

The slight decrease in the rate constants towards higher energies might be explained by the passage of photoelectrons through the crystal. Calculations using the computer program *CASINO* (Hovington *et al.*, 1997) show that when the energy increases from 7.0 to 15.0 keV the average distance travelled by a photoelectron inside the crystal increases from approximately 0.6 to 2.5 µm. Thus, photoelectrons might leave the thin crystal plates and deposit part of their energy outside (Nave & Hill, 2005). This might result in lower actual doses. Moreover, the cryoprotectant film also interacts with the photoelectrons, an effect that is not accounted for by the dose calculation (Murray *et al.*, 2004).

3.1.2. Radical scavengers. Radical scavengers have been discussed as a possible means to reducing secondary radiation damage. These compounds can be introduced into the crystal lattice by soaking or co-crystallization. Suggested scavengers include ascorbate (Murray & Garman, 2002; Buxton *et al.*, 1988; O'Neill *et al.*, 2002), glucose, glycerol, *t*-butanol, styrene (Zaloga *et al.*, 1974; Murray & Garman, 2002), nicotinic acid (Kauffmann *et al.*, 2006) and sodium nitrate (Makarov *et al.*, 1969). These molecules might react with radical species and thus prevent their interaction with the protein molecules in the crystal, effectively protecting the macromolecule from secondary damage events. Initial measurements showed that high concentrations of ascorbate (ninefold molar excess over protein) can prevent breakage of disulfide bridges in lysozyme crystals that absorbed a radiation dose of 8 MGy (Murray & Garman, 2002). Kauffmann *et al.* (2006) analyzed the effect of radical scavengers on radiation damage to crystals of different proteins, but did not report the dose, which makes a quantitative comparison difficult.

Ascorbate. Ascorbate is a scavenger for $OH^{\bullet}$ radicals that also serves as an antioxidant (Buxton *et al.*, 1988). Therefore, it is reasonable to assume that the addition of ascorbate should influence the rate of radiolytic reduction. Myoglobin crystals of equal size (~200 µm × 100 µm × 4 µm) were soaked for ~120 s in cryoprotectant solutions containing 0.0, 0.15 or 0.3 *M* sodium ascorbate. This corresponds to no, 7.5- and 15-fold molar excess of ascorbate over myoglobin, respectively. The crystals were irradiated with 12 keV X-rays and a flux of 5.6×10^9 photons s^{-1} with simultaneous acquisition of optical spectra. As energy, flux and absorption probability stayed the same for all samples, the rate constants do not have to be normalized. As shown in Fig. 3, both rate constants are effected by the addition of ascorbate. A concentration of 0.15 *M* sodium ascorbate reduces k_1 by 40%, while k_2 is reduced by only 25%. Further addition of ascorbate seems to have only a slightly reducing effect on k_2 and none on k_1 which is in line with the proposed origin of the processes described above.

Glycerol. Glycerol is a widely used cryoprotectant in crystallographic and in optical studies owing to its ability to form

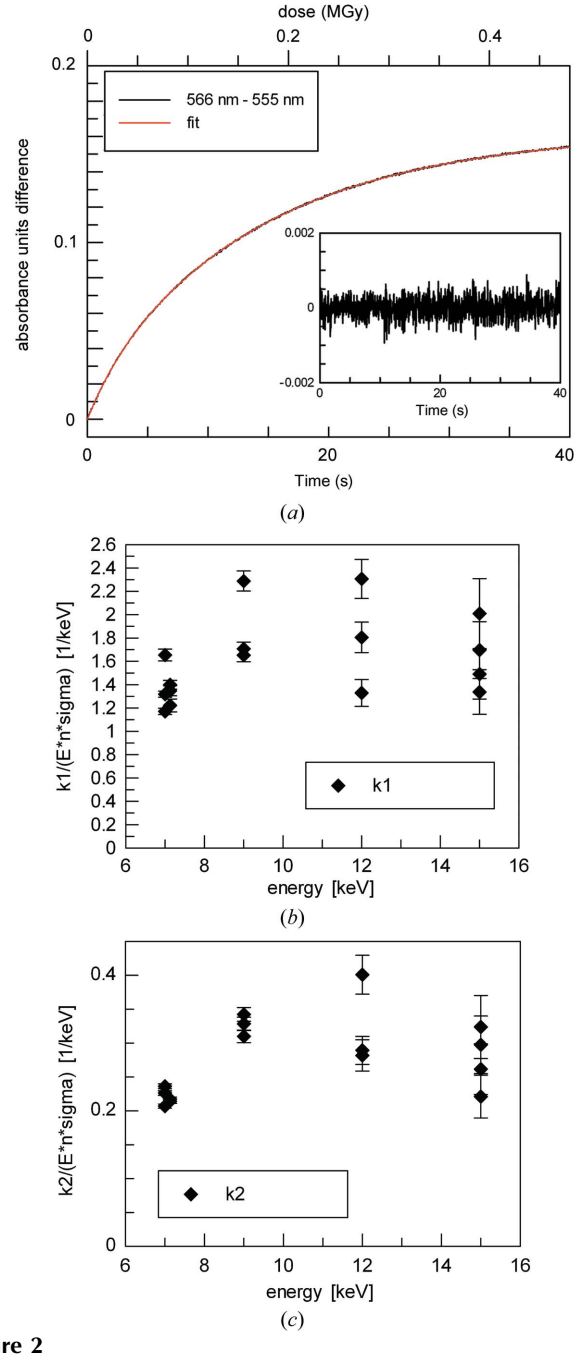

Figure 2
(*a*) Time course of the absorption difference between the peaks at 566 nm and 555 nm following exposure to 7 keV X-rays superimposed by the fit (red) used for generating parts (*b*) and (*c*). Inset: residuals of the fit. (*b*) Energy dependence of the cryoradiolytic reduction rate k_1 of ferric (Fe^{3+}) myoglobin to ferrous (Fe^{2+}) myoglobin. (*c*) Energy dependence of the rate constant k_2.

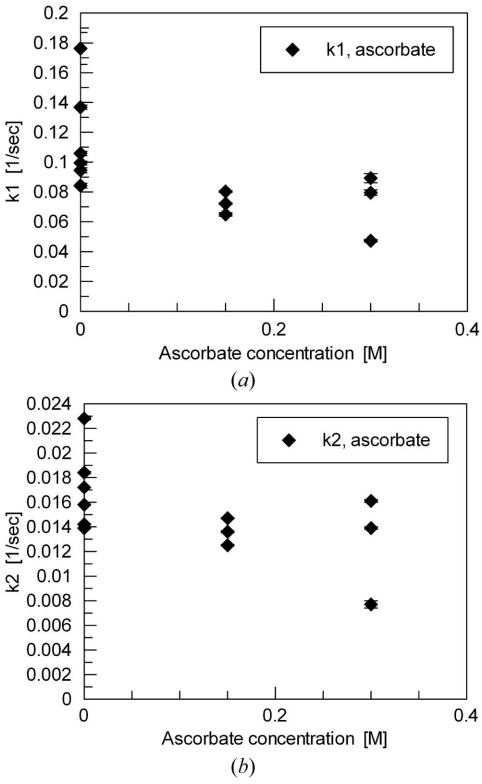

Figure 3
Dependence of the reduction rates k_1 (*a*) and k_2 (*b*) of ferric (Fe^{3+}) myoglobin to ferrous (Fe^{2+}) myoglobin on the ascorbate concentration in the cryoprotectant solution, obtained from the time evolution of the absorption difference between the 566 nm and 555 nm bands. No influence on the reduction rate is observed.

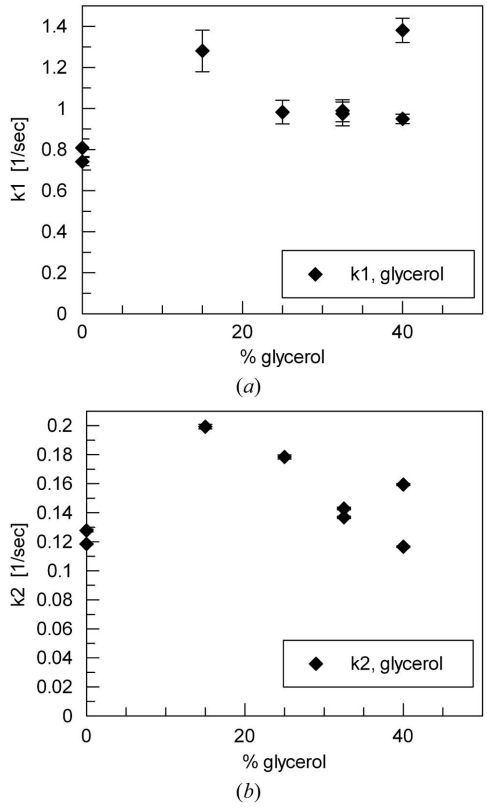

Figure 4
Influence of the glycerol concentration on the rates k_1 (*a*) and k_2 (*b*) of the reduction of ferric (Fe^{3+}) myoglobin to ferrous (Fe^{2+}) myoglobin at 100 K, derived from the time evolution of the absorption difference between the 566 nm and 555 nm bands. The rate constants of 0 and 40% glycerol were normalized for σ to fit the other rate constants. The rates decrease at higher glycerol concentrations.

transparent glasses when cryocooled. Moreover, glycerol has been widely discussed as a radical scavenger (O'Neill *et al.*, 2002). Therefore, glycerol has been implicated as the cause for the difference in reduction yield of ribonucleotide reductase observed in various experiments (Davydov *et al.*, 1994), since it can scavenge mobile electron holes. Hendrich *et al.* used no glycerol, radiation from a Mo-target X-ray tube and observed hardly any (0.5%) reduction (Hendrich *et al.*, 1991). Davydov *et al.* used 50% glycerol, γ-radiation from a ^{137}Cs source and observed a 50% yield of mixed-valent (Fe^{3+}/Fe^{2+}) states (Davydov *et al.*, 1994). A structural study by Eklund and co-workers reported reduction of ribonucleotide reductase crystals by synchrotron radiation (14.8 keV, beamline BW7B, EMBL c/o DESY, Hamburg) when using 20% glycerol as cryoprotectant, but none when using 15% PEG 400 as cryoprotectant (Eriksson *et al.*, 1998). The latter study is the only one comparing experiments that seem to differ in only one variable, the glycerol concentration. However, no dose was reported.

To probe the influence of glycerol on radiolytic reduction rates and yields, we soaked myoglobin crystals with cryoprotectant solutions containing different concentrations of glycerol. To retain the composition of the solutions, we chose 100 m*M* sodium citrate buffer, pH 5.0, and 2.2 *M* ammonium sulfate with 0, 15, 25, 32.5 and 40% glycerol. To achieve cryoprotection for the 0% glycerol sample, the ammonium sulfate concentration was increased to 3.5 *M*. In the case of 40% glycerol, the ammonium sulfate concentration was decreased to 2.0 *M* owing to precipitation. The experiment was carried out at 13 keV. As can be seen in Fig. 4, the rate constants show a modest, but incomplete, dependency on the glycerol concentration. The rate constant k_1 increases with addition of glycerol between 0 and 15% and stays constant at an intermediate value for higher glycerol concentrations. The reduction rate constant k_2, on the other hand, decreases moderately between 15 and 40% glycerol. Interestingly, also for k_2, reduction was even slower without glycerol. This would be in line with the findings on ribonucleotide reductase (Eriksson *et al.*, 1998). The deviation of the data points at 0% glycerol is probably due to the high ammonium sulfate concentration. It is known that high concentrations of SO_4^{2-} ions yield high amounts of $SO_4^{2-\bullet}$ radicals that act as a strong electron acceptor (Burmeister, 2000).

Sodium nitrate. Sodium nitrate is known as a scavenger for hydrated electrons (Makarov *et al.*, 1969; Fukumura *et al.*, 2003). Myoglobin crystals of equal size ($\sim$200 µm $\times$ 100 µm $\times$ 4 µm) were soaked in cryopotection solutions for $\sim$120 s with 0, 0.15 or 0.3 *M* sodium nitrate. The crystals were irradiated with 12 keV X-rays and a flux of 5.6×10^9 photons s^{-1} with simultaneous acquisition of optical spectra. The rate constant k_1 (Fig. 5*a*) shows a decrease between 0 and 0.15 *M* scavenger concentration and flattens towards higher concentrations.

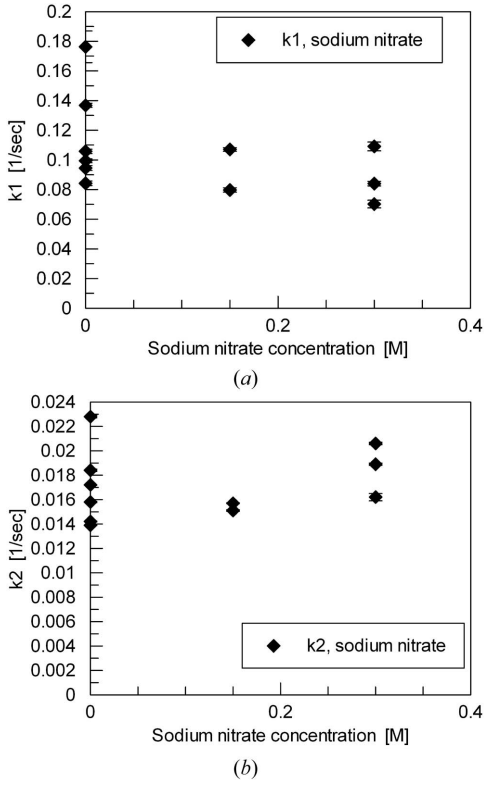

Figure 5
Dependence of the reduction rates k_1 (*a*) and k_2 (*b*) of ferric (Fe^{3+}) myoglobin to ferrous (Fe^{2+}) myoglobin on the sodium nitrate concentration in the cryoprotectant solution, obtained from the time evolution of the absorption difference between the 566 nm and 555 nm bands.

Interestingly, k_2 (Fig. 5*b*) seems slightly decreased between 0 and 0.15 *M* sodium nitrate but increases again at 0.3 *M*.

Nicotinamide. Nicotinic acid has been found to be a good scavenger to reduce radiation damage (Kauffmann *et al.*, 2006). As nicotinamide does not differ from nicotinic acid in the important aspects such as molecule size, chemical properties (aromatic system) and solubility, we analysed the effect of this molecule. Myoglobin crystals of equal size (~200 µm × 100 µm × 4 µm) were prepared and examined analogous to the data collected for sodium ascorbate and sodium nitrate. Interestingly, the addition of nicotinamide changed the absorbance spectra of the non-irradiated as well as the radio-reduced myoglobin crystals somewhat (Fig. 6*a*). This suggests an interaction of the molecule with the heme group, which might have implications for the reduction rates of the iron ion. This can be seen in the rate constant k_1 (Fig. 6*b*) which, instead of decreasing, as in the case of sodium ascorbate or sodium nitrate, increases by almost 50% between 0 and 0.15 *M* nicotinamide but drops down again at 0.3 *M*. On the other hand, k_2 (Fig. 6*c*) stays constant between 0 and 0.15 *M* nicotinamide but decreases towards higher concentrations. To verify this strong dependence it is necessary to replicate these experiments with concentrations between 0 and 0.15 *M* nicotinamide as well as concentrations higher than 0.3 *M* and for other heme proteins that show no interaction with nicotinamide.

Qualitatively, the protecting effect of nicotinamide agrees with the findings reported by Kauffmann *et al.* (2006), who

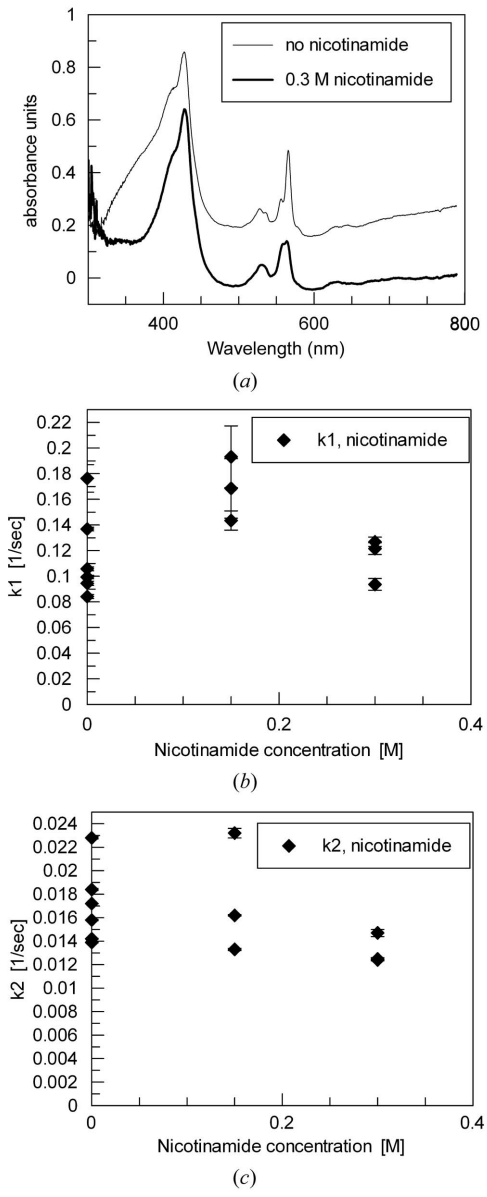

Figure 6
(*a*) Spectra of irradiated myoglobin crystals with and without nicotinamide. (*b*), (*c*) Dependence of the reduction rates k_1 (*b*) and k_2 (*c*) of ferric (Fe^{3+}) myoglobin to ferrous (Fe^{2+}) myoglobin on the nicotinamide concentration in the cryoprotectant solution, obtained from the time evolution of the absorption difference between the 566 nm and 555 nm bands.

analyzed the influence of 200 m*M* nicotinic acid on the diffraction qualities and the persistence of disulfide bridges and carboxylate side chains in lysozyme, thaumatin and porcine pancreatic elastase crystals. However, no dose values were given.

3.2. Cytochrome P450cam

Cytochrome P450 enzymes are mono-oxygenases that are unique in their ability to hydroxylate non-activated hydrocarbons. P450s activate molecular oxygen by a sequential two-electron reduction that involves the following steps (reviewed by Denisov *et al.*, 2005): molecular oxygen binds to the

reduced heme iron and forms an oxygenated heme Fe^{2+}-OO or Fe^{3+}-OO^{-} complex, the one-electron reduction of this oxy complex yields a ferric peroxo Fe^{3+}-OO^{2-} complex, which is protonated to form the hydroperoxo Fe^{3+}-OOH^{-} species. The second protonation of the distal oxygen atom results in heterolytic scission of the O—O bond under formation of a water molecule and the generation of a fleeting ferryl-oxo π-cation porphyrin radical intermediate. This is referred to as 'Compound I' and is believed to be the active oxygen species in hydroxylation reactions. The oxy complex is the last stable intermediate along the reaction coordinate; in P450cam it has a half life of ~10 min at 277 K (Sligar *et al.*, 1974). The subsequent peroxo and hydroperoxy intermediates have only been observed recently by cryoradiolytic reduction of oxyferrous P450 using ^{60}Co or ^{32}P sources for the generation of photoelectrons (reviewed by Denisov *et al.*, 2002*b*). Following irradiation of the cryotrapped oxyferrous complex the temperature was raised transiently, then the sample was cooled again and analyzed by UV-Vis, ^{1}H-ENDOR and EPR spectroscopy (Denisov *et al.*, 2001; Davydov *et al.*, 2001). This protocol was followed to temperatures above the glass transition temperature. When keeping the sample at 6 K, a hydrogen-bonded peroxo species was observed. In the wild-type enzyme, it converts largely to the hydroperoxo complex at ~70 K, and does so completely at temperatures near ~147 K (Davydov *et al.*, 2001).

The crystal structure of oxyferrous P450cam has been determined. In contrast to a recent study (Nagano & Poulos, 2005) the first report (Schlichting *et al.*, 2000) noted an X-ray wavelength-dependent decay of the electron density of the heme-bound oxygen molecule. In particular, irradiation with 1.5 Å X-rays (~8.3 keV) resulted in a decrease of the electron density corresponding to the distal oxygen atom of the heme-bound O_2. This complex was tentatively assigned to an oxy-ferryl species. Transient thawing of the crystal resulted in formation of the 5-hydroxycamphor product complex, implying that the preceding intermediate was on the reaction coordinate. This, in turn, means that the crystalline oxyferrous complex turns over to the peroxo and hydroperoxo complexes, in analogy to the radiolytic annealing experiments on frozen solutions mentioned above. On the one hand, this opens the possibility to generate, enrich and (structurally) characterize the fleeting reaction intermediates, whereas, on the other hand, it casts some doubts on the identity of the crystal structures of the oxyferrous complexes. To explore both possibilities, we irradiated monoclinic oxyferrous P450cam crystals (thickness 50 µm) with 13 keV X-rays (the flux was 9.3×10^{11} photons s^{-1} within an area of 100 µm × 120 µm FWHM, yielding a dose rate of 0.029 MGy s^{-1}). The temporal evolution of the optical spectra of oxyferrous P450cam crystals kept at 140 K during X-ray exposure is shown in Fig. 7. The crystal contains a mixture of the binary ferric camphor complex (Soret band at ~377 nm) and the ternary oxyferrous camphor complex (Soret band at ~426 nm). Within 1 s (0.029 MGy), the 426 nm Soret band shifts towards the red to 444 nm and the associated *Q* bands form new peaks at 545 nm and 562 nm. This is consistent with the formation of the ferric

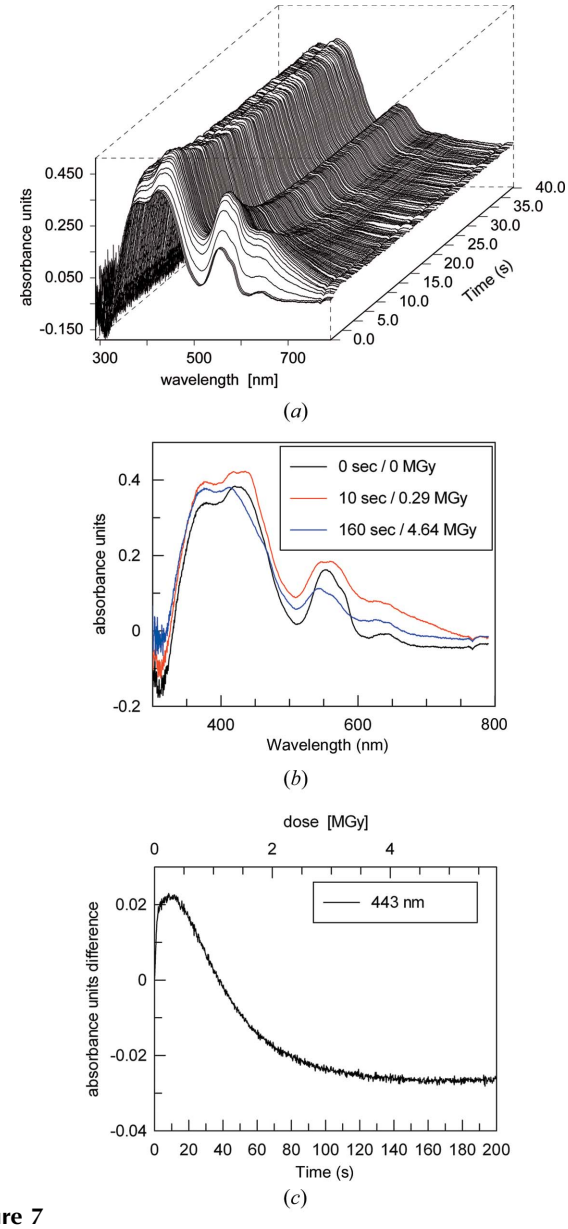

Figure 7
Cryoradiolytic reduction of an oxyferrous cytochrome P450cam crystal at 140 K. (*a*) UV-Vis absorption spectra of P450cam during irradiation with an unfocused X-ray beam. New peaks at 443 and 563 nm are formed, and the Soret band shifts first to the red (hydroperoxo complex formation), then to the blue (reduction). (*b*) UV-Vis spectra after different times of irradiation. (*c*) Time course of the 443 nm peak. To obtain only the height of the peak, the arithmetic mean of the absorbances at 426 nm and 459 nm was subtracted (see Fig. 8*a*).

hydroperoxo complex (Makris *et al.*, 2004). This complex decays over the next 5 s (0.174 MGy) to the reduced ferrous complex, which is characterized by a strongly blue-shifted Soret band (~410 nm). Also the 562 nm band decays slowly to leave only the 543 nm peak and a shoulder at 564 nm.

3.2.1. Solvated electrons and radicals. During irradiation, a variety of radicals are formed, in particular $OH^{\bullet}$ and $H^{\bullet}$ radicals, as well as solvated electrons. For certain cryoprotectant solutions the formation of solvated electrons can be monitored through the blue–purple or sometimes even reddish colour of the irradiated area. This colour can be

photobleached by either further irradiation or through illumination with UV light. Additionally, the persistence of the absorption depends on temperature. Fig. 8(*a*) shows a series of difference absorption spectra of a P450cam crystal during irradiation with X-rays of 13 keV at 140 K. The formation of a solvated electron spectrum is visible during the first second. Subsequently, the spectrum decays within 20 s. The presence of electrons can also be monitored by following the absorbance at 676 nm (Fig. 8*c*), which is clearly within the electron absorption spectrum (Eiben & Taub, 1967; Willard, 1973) and does not interact with features of the underlying P450 species. The formation of radicals can be observed by following the absorption at 321 nm. The true composition of radicals present is still unknown even though absorbance spectra of possible low-molecular-weight analogs have been studied in solution (Jonah & Rao, 2001). At least part of this absorbance is due to H and OH radicals. These two radical species have overlying absorbance spectra peaking at 280 nm (Ghormley & Stewart, 1956). As light output of the xenon light source was low in this region, we chose 321 nm for our analysis as the temporal evolution was still observable despite the noise of the absorbance signal. The creation follows a linear dependence with absorbed dose. During irradiation, solvated electrons can travel through the sample. At some point they can be absorbed by a radical or another electron acceptor. Radicals, on the other hand, are immobile at cryogenic temperatures and remain at the position of their creation. They accumulate in the irradiated volume and newly generated electrons are likely to combine with one of these radicals if their energy is too low to travel further away. Because of this and possibly because of tunnelling (Miller, 1972), the number of solvated electrons decreases after a short while and reaches a steady-state plateau with equal rates of formation and recombination, while the concentration of radicals increases linearly (Fig. 8*b*) (see also Ekstrom *et al.*, 1970).

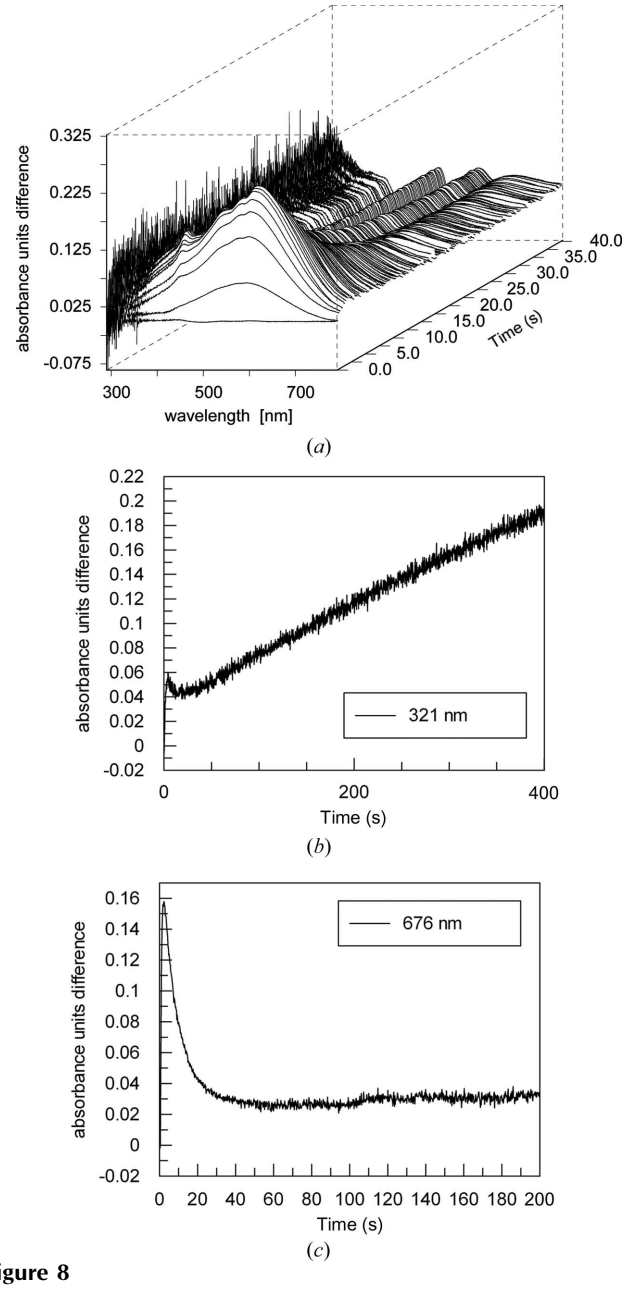

Figure 8
UV-Vis absorption spectra of trapped electrons and radicals induced by X-ray irradiation. (*a*) Difference spectra between absorption spectra of an oxyferrous P450cam crystal before and during irradiation. The creation and decay of a broad spectrum of trapped solvated electrons within the first few seconds can be observed. Spectra were acquired with a time interval of 0.2 s. (*b*) The concentration of radicals, absorbing at 321 nm, increases linearly with time. At the beginning there is an overlap with the absorption band associated with the trapped electrons. (*c*) In contrast, the concentration of trapped solvated electrons, which absorb at 676 nm, increases quickly and decays again.

3.3. Chloroperoxidase

Chloroperoxidase (CPO) is a heme-thiolate enzyme catalyzing hydrogen-peroxide-dependent halogenation reactions. In the ground state of the enzyme, the ferric heme iron (Fe^{3+}) is hexa-coordinated and in the low-spin state (Liu *et al.*, 1995). EXAFS studies of ferric chloroperoxidase yielded a distance of 2.1 Å between the ferric iron and the water molecule that serves as the sixth ligand (Green *et al.*, 2004). Yet, we observed a much larger distance (3.5 Å) between iron and water in the recently determined structures of CPO crystallized in the presence of either bromide or iodide [Protein Data Bank (PDB) accession codes: 2ciw, 2civ (Kühnel *et al.*, 2006)]. These high-resolution diffraction data were collected at a third-generation synchrotron X-ray source with the crystals kept at 100 K, but a distance of 3.4 Å was also reported for a previously published CPO structure using data from a crystal kept at room temperature and collected with a rotating-anode generator equipped with focusing optics [PDB accession code: 1cpo (Sundaramoorthy *et al.*, 1995)]. The large distance between the iron and water indicates that the ferric iron was reduced to the ferrous state by the electrons released during data collection, yielding the penta-coordinated high-spin state of the enzyme. Since we wanted to investigate how quickly the reduction occurs, absorption spectra of CPO crystals were recorded while exposing them to X-rays with an energy of 12 keV (Fig. 9). Within seconds of X-ray irradiation, a new peak appears at 563 nm (Figs. 9*a* and 9*b*), which corresponds

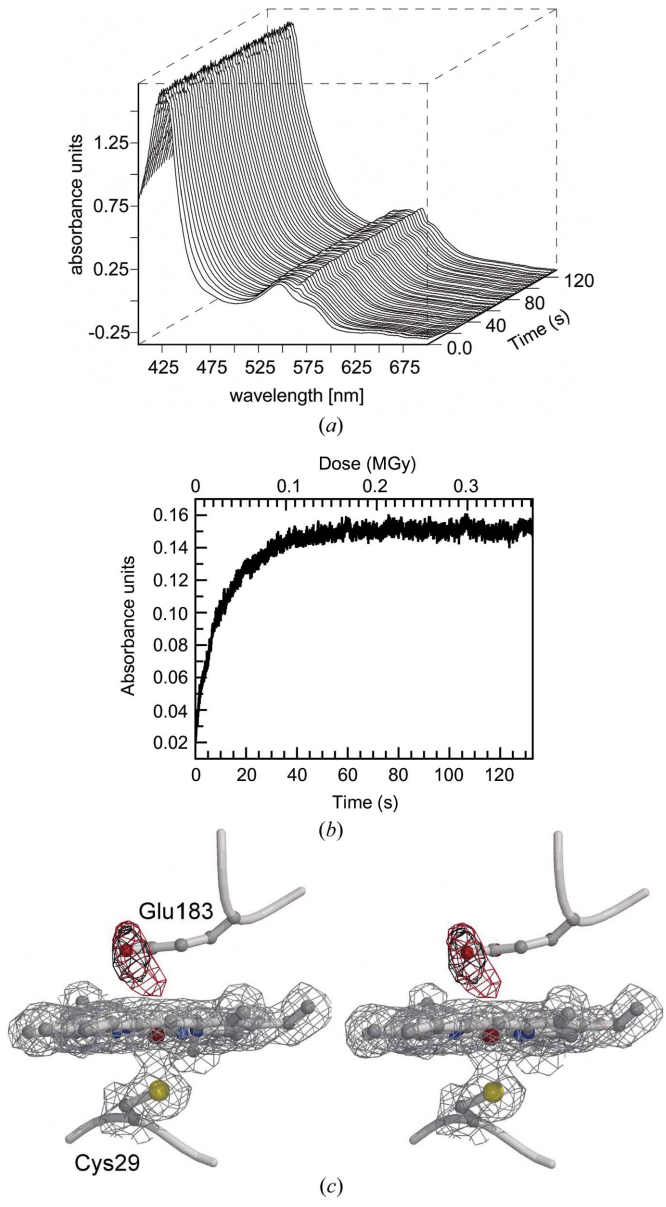

Figure 9
Cryoradiolytic reduction of chloroperoxidase. (*a*) UV-Vis spectra of CPO crystals recorded during X-ray exposure at 12 keV with a flux of 6.3×10^{10} photons s^{-1}, yielding a dose rate of 0.028 MGy s^{-1}. The beam was defocused to 100 µm × 100 µm and two 200 µm Al absorbers were inserted. A new peak at 563 nm rapidly appears. No shift of the Soret band is observed. (*b*) Time and dose dependency of peak formation at 563 nm. (*c*) Active site of CPO. The 1.75 Å resolution σA-weighted $2mF_o - DF_C$ map is shown in grey with a contour level of 1σ. The $mF_o - DF_c$ omit map of the low-dose data set is shown in red and the corresponding density of the high-dose data set is drawn in black. Both difference maps are contoured at 3σ.

to the peak at 550 nm observed in ferrous CPO solutions, when the enzyme is chemically reduced with dithionate (Lambeir & Dunford, 1985; Morris & Hager, 1966). Cryoradiolytic reduction of CPO solutions with ^{60}Co γ-radiation at 77 K also yields formation of the 563 nm peak and a shift of the Soret band from 400 nm to 438 nm (Metodiewa & Dunford, 1990). We did not observe a shift of the 426 nm Soret peak in the crystal spectra.

Table 1
Crystallographic data collection and refinement statistics.

	CPO low dose	CPO high dose
PDB accession code	2j18	2j19
Space group	$C222_1$	$C222_1$
Unit-cell dimensions *a*, *b*, *c* (Å)	57.7, 150.5, 100.8	57.7, 150.5, 100.8
Beamline/X-ray source	SLS X10SA	SLS X10SA
Wavelength (Å)	0.9761	0.9761
Resolution of data (Å) (high-resolution bin)	20–1.75 (1.80–1.75)	20–1.75 (1.80–1.75)
No. of observations/ unique reflections	185512/43164	190444/43278
Completeness total (high) (%)	95.5 (95.3)	95.3 (94.1)
$I/\sigma I$ total (high)	10.9 (6.3)	10.8 (5.8)
R_{sym} total (high) (%)	13.2 (38.9)	14.1 (54.6)
Wilson *B*-factor (Å^2)	19.7	20.8
Refinement		
R_{work}/R_{free} (%)	17.4/20.6	17.6/20.4
Protein residues (number of atoms)	298 (2316)	298 (2316)
Sugar residues (number of atoms)	17 (202)	17 (202)
Water	359	340
Ligands (total number of atoms)	3 Br heme (43)	3 Br heme (43)
Overall *B*-factor (Å^2)	14.3	15.9
r.m.s. deviations		
Bond length (Å)	0.012	0.011
Bond angles (°)	1.38	1.41

We employed a multi-crystal composite data-collection strategy in order to compare 'low dose' and 'high dose' CPO crystal structures (for details see §2). The resolution of the two merged data sets is 1.75 Å (Fig. 9*c*, Table 1). During data collection of the low-dose data set, the crystals received a dose of 0.5 MGy, as calculated using *RADDOSE* (Murray *et al.*, 2004), whereas after collection of the second data set the crystals have absorbed an approximate tenfold higher X-ray dose (5.9 MGy), still well below the dose limit of 30 MGy (Owen *et al.*, 2006). In the low-dose data set an elongated density is observed above the heme, which is not continuous to the heme iron (Fig. 9*c*). This density was modelled as a single water molecule at two positions, with distances to the iron of 2.6 Å and 4.2 Å, respectively. This indicates that a mixture of ferric/ferrous CPO is present already in the low-dose structure. In contrast, in the high-dose structure, CPO is completely reduced to the ferrous state, and a round density, fitting a single water molecule, is located 3.6 Å away from the iron. The second significant change is the cleavage of the single disulfide bridge (Cys79–Cys86) in the structure refined against the high-dose data set, whereas this bond is intact in the low-dose structure. The sensitivity of disulfide bridges towards radiation is well known (Weik *et al.*, 2000; Burmeister, 2000; Ravelli & McSweeney, 2000).

In conclusion, the reduction of the CPO crystals occurs so rapidly ($k = 0.10 \pm 0.01$ s^{-1}) that even with a composite data-collection strategy only a mixture of the ferric and ferrous states could be observed. The CPO structures deposited in the Protein Data Bank do not represent the ferric ground state but rather the reduced ferrous enzyme.

4. Concluding remarks

The findings presented here reveal the unexpectedly rapid photoreduction of three different heme proteins that differ markedly in amino acid composition, reduction potential [CPO: +150 mV (pH 2.7) (Makino *et al.*, 1976), myoglobin +59 mV (Varadarajan *et al.*, 1989); P450cam: −170 mV (Fisher & Sligar, 1985)] and active-site chemistry. In all cases the dose required for photoreduction was accumulated within the experimental settings corresponding only to roughly a dozen degrees worth of rotation data. On average, the addition of electron or radical scavenging compounds slows the reduction by some 20%. Although this effect is significant, it is much smaller than the increase in protection against breakage of disulfide bridges or decarboxylations reported in 'regular' radiation damage experiments (Murray & Garman, 2002; Kauffmann *et al.*, 2006). It would seem as if the heme iron acts as some kind of 'vacuum cleaner', sucking in electrons. This emphasizes the importance of microspectroscopic determination of the dose allowed for data collection before the species under investigation turns over into a new one (Kühnel *et al.*, 2007). Our results strongly emphasize the previously raised concern about the actual oxidation state of many redox proteins in the Protein Data Bank (Berglund *et al.*, 2002).

We are grateful to Ehmke Pohl, Anuschka Pauluhn, Alke Meents and Roman Schneider for help in setting up the experiment at the SLS, and Georg Holtermann (MPI Dortmund) for the design of the microspectrophotometer holder. We thank James Terner (Virginia Commonwealth University, Richmond) for the CPO used in this study, Jochen Reinstein, Ilia G. Denisov (University of Illinois Urbana-Champaign) and Edgar Weckert (DESY Hamburg) for stimulating discussions, and acknowledge funding by the DFG (SFB 623).

References

Adam, V., Royant, A., Niviere, V., Molina-Heredia, F. P. & Bourgeois, D. (2004). *Structure*, **12**, 1729–1740.
Berglund, G. I., Carlsson, G. H., Smith, A. T., Szoke, H., Henriksen, A. & Hajdu, J. (2002). *Nature (London)*, **417**, 463–468.
Blake, C. C. F. & Phillips, D. C. (1962). *Symposium on the Biological Effects of Ionizing Radiation at the Molecular Level.* Vienna: International Atomic Energy Agency.
Blanke, S. R., Yi, S. & Hager, L. P. (1989). *Biotechnology Lett.* **11**, 769–774.
Bourgeois, D., Vernede, X., Adam, V., Fioravanti, E. & Ursby, T. (2002). *J. Appl. Cryst.* **35**, 319–326.
Burmeister, W. P. (2000). *Acta Cryst.* D**56**, 328–341.
Buxton, G. V., Clive, L., Greenstock, W., Helman, P. & Ross, A. B. (1988). *J. Phys. Chem. Ref. Data*, **17**, 513–886.
Carugo, O. & Carugo, K. D. (2005). *Trends Biochem. Sci.* **30**, 213–219.
Champloy, F., Gruber, K., Jogl, G. & Kratky, C. (2000). *J. Synchrotron Rad.* **7**, 267–273.
Chance, B., Angiolillo, P., Yang, E. K. & Powers, L. (1980). *FEBS Lett.* **112**, 178–182.
Crosson, S. & Moffat, K. (2002). *Plant Cell*, **14**, 1067–1075.
Davydov, R., Kuprin, S., Graslund, A. & Ehrenberg, A. (1994). *J. Am. Chem. Soc.* **116**, 11120–11128.
Davydov, R., Ledbetter-Rogers, A., Martasek, P., Larukhin, M., Sono, M., Dawson, J. H., Masters, B. S. S. & Hoffman, B. M. (2002). *Biochemistry*, **41**, 10375–10381.
Davydov, R., Macdonald, I. D. G., Makris, T. M., Sligar, S. G. & Hoffman, B. M. (1999). *J. Am. Chem. Soc.* **121**, 10654–10655.
Davydov, R., Makris, T. M., Kofman, V., Werst, D. E., Sligar, S. G. & Hoffman, B. M. (2001). *J. Am. Chem. Soc.* **123**, 1403–1415.
Davydov, R. M., Yoshida, T., Ikeda-Saito, M. & Hoffman, B. M. (1999). *J. Am. Chem. Soc.* **121**, 10656–10657.
Denisov, I. G., Makris, T. M. & Sligar, S. G. (2001). *J. Biol. Chem.* **276**, 11648–11652.
Denisov, I. G., Makris, T. M. & Sligar, S. G. (2002*a*). *J. Biol. Chem.* **277**, 42706–42710.
Denisov, I. G., Makris, T. M. & Sligar, S. G. (2002*b*). *Methods Enzymol.* **357**, 103–115.
Denisov, I. G., Makris, T. M., Sligar, S. G. & Schlichting, I. (2005). *Chem. Rev.* **105**, 2253–2277.
Denisov, I. G., Victoria, D. C. & Sligar, S. G. (2007). *Radiat. Phys. Chem.* In the press.
Eaton, W. A. & Hofrichter, J. (1981). *Methods Enzymol.* **76**, 175–261.
Eiben, K. & Taub, I. A. (1967). *Nature (London)*, **216**, 782–783.
Ekstrom, A., Suenram, R. & Willard, J. E. (1970). *J. Phys. Chem.* **74**, 1888–1894.
Emsley, P. & Cowtan, K. (2004). *Acta Cryst.* D**60**, 2126–2132.
Ericson, A., Hedman, B., Hodgson, K. O., Green, J., Dalton, H., Bentsen, J. G., Beer, R. H. & Lippard, S. J. (1988). *J. Am. Chem. Soc.* **110**, 2330–2332.
Eriksson, M., Jordan, A. & Eklund, H. (1998). *Biochemistry*, **37**, 13359–13369.
Fedorov, R., Schlichting, I., Hartmann, E., Domratcheva, T., Fuhrmann, M. & Hegemann, P. (2003). *Biophys. J.* **84**, 2474–2482.
Fisher, M. T. & Sligar, S. G. (1985). *J. Am. Chem. Soc.* **107**, 5018–5019.
Fukumura, T., Akaike, S., Yoshida, Y. & Suzuki, K. (2003). *Nucl. Med. Biol.* **30**, 389–395.
Garman, E. F. & Owen, R. L. (2006). *Acta Cryst.* D**62**, 32–47.
Ghormley, J. A. & Stewart, A. C. (1956). *J. Am. Chem. Soc.* **78**, 2934–2939.
Green, M. T., Dawson, J. H. & Gray, H. B. (2004). *Science*, **304**, 1653–1656.
Hadfield, A. & Hajdu, J. (1993). *J. Appl. Cryst.* **26**, 839–842.
Hendrich, M. P., Elgren, T. E. & Que, L. Jr (1991). *Biochem. Biophys. Res. Commun.* **176**, 705–710.
Hovington, P., Drouin, D. & Gauvin, R. (1997). *Scanning*, **19**, 1–14.
Jonah, C. D. & Rao, B. S. M. (2001). *Radiation Chemistry. Present Status and Future Trends. Studies in Physical and Theoretical Chemistry.* Amsterdam: Elsevier.
Jones, G. D., Lea, J. S., Symons, M. C. & Taiwo, F. A. (1987). *Nature (London)*, **330**, 772–773.
Kabsch, W. (1993). *J. Appl. Cryst.* **26**, 795–800.
Kauffmann, B., Weiss, M. S., Lamzin, V. S. & Schmidt, A. (2006). *Structure*, **14**, 1099–1105.
Klapper, M. H. & Faraggi, M. (1979). *Q. Rev. Biophys.* **12**, 465–519.
Kort, R., Komori, H., Adachi, S., Miki, K. & Eker, A. (2004). *Acta Cryst.* D**60**, 1205–1213.
Kühnel, K., Blankenfeldt, W., Terner, W. & Schlichting, I. (2006). *J. Biol. Chem.* **281**, 23990–23998.
Kühnel, K., Derat, E., Terner, J., Shaik, S. & Schlichting, I. (2007). *Proc. Natl. Acad. Sci. USA*. In the press.
Lamb, D. C., Ostermann, A., Prusakov, V. E. & Parak, F. G. (1998). *Eur. Biophys. J.* **27**, 113–125.
Lambeir, A. M. & Dunford, H. B. (1985). *Eur. J. Biochem.* **147**, 93–96.
Liu, H. I., Sono, M., Kadkhodayan, S., Hager, L. P., Hedman, B., Hodgson, K. O. & Dawson, J. H. (1995). *J. Biol. Chem.* **270**, 10544–10550.
Makarov, I. E., Ershov, B. G. & Pikaev, A. K. (1969). *Izv. Akad. Nauk SSSR, Chem. (Engl. Transl.)*, **10**, 2170–2175.
Makino, R., Chiang, R. & Hager, L. P. (1976). *Biochemistry*, **15**, 4748–4754.

Makris, T., Denisov, I., Schlichting, I. & Sligar, S. G. (2004). *Cytochrome P450: Structure, Mechanism and Biochemistry*, 3rd ed., edited by P. R. Ortiz de Montellano, pp. 149–182. New York: Kluwer Academic/Plenum.
Mees, A., Klar, T., Gnau, P., Hennecke, U., Eker, A. P. M., Carell, T. & Essen, L. O. (2004). *Science*, **306**, 1789–1793.
Metodiewa, D. & Dunford, H. B. (1990). *Biochem. Biophys. Res. Commun.* **168**, 1311–1317.
Miller, J. R. (1972). *J. Chem. Phys.* **56**, 5173–5183.
Moan, J. & Kaalhus, O. (1973). *Int. J. Radiat. Phys. Chem.* **5**, 441–451.
Morris, D. R. & Hager, L. P. (1966). *J. Biol. Chem.* **241**, 1763–1768.
Mozumder, A. & Magee, J. L. (1966). *Radiat. Res.* **28**, 203–214.
Murray, J. W. & Garman, E. F. (2002). *J. Synchrotron Rad.* **9**, 347–354.
Murray, J. W., Garman, E. F. & Ravelli, R. B. G. (2004). *J. Appl. Cryst.* **37**, 513–522.
Murray, J. W., Rudiño-Piñera, E., Owen, R. L., Grininger, M., Ravelli, R. B. G. & Garman, E. F. (2005). *J. Synchrotron Rad.* **12**, 268–275.
Murshudov, G. N., Vagin, A. A., Lebedev, A., Wilson, K. S. & Dodson, E. J. (1999). *Acta Cryst.* D**55**, 247–255.
Nagano, S. & Poulos, T. L. (2005). *J. Biol. Chem.* **280**, 31659–31663.
Navaza, J. (2001). *Acta Cryst.* D**57**, 1367–1372.
Nave, C. (1995). *Radiat. Phys. Chem.* **45**, 483–490.
Nave, C. & Hill, M. A. (2005). *J. Synchrotron Rad.* **12**, 299–303.
O'Neill, P., Stevens, D. L. & Garman, E. F. (2002). *J. Synchrotron Rad.* **9**, 329–332.
Owen, R. L., Rudiño-Piñera, E. & Garman, E. F. (2006). *Proc. Natl. Acad. Sci. USA*, **103**, 4912–4917.
Pearson, A. R., Mozzarelli, A. & Rossi, G. L. (2004). *Curr. Opin. Struct. Biol.* **14**, 656–662.
Penner-Hahn, J. E., Murata, M., Hodgson, K. O. & Freeman, H. C. (1989). *Inorg. Chem.* **28**, 1826–1832.
Pohl, E., Pradervand, C., Schneider, R., Tomizaki, T., Pauluhn, A., Chen, Q., Ingold, G., Zimoch, E. & Schulze-Briese, C. (2006). *Synchrotron Rad. News*, **19**, 24–26.
Prusakov, V. E., Steyer, J. & Parak, F. G. (1995). *Biophys J.* **68**, 2524–2530.
Ravelli, R. B. G. & McSweeney, S. M. (2000). *Structure*, **8**, 315–328.
Sakai, K., Matsui, Y., Kouyama, T., Shiro, Y. & Adachi, S. (2002). *J. Appl. Cryst.* **35**, 270–273.
Sato, M., Shibata, N., Morimoto, Y., Takayama, Y., Ozawa, K., Akutsu, H., Higuchi, Y. & Yasuoka, N. (2004). *J. Synchrotron Rad.* **11**, 113–116.
Schlichting, I., Berendzen, J., Chu, K., Stock, A. M., Maves, S. A., Benson, D. E., Sweet, R. M., Ringe, D., Petsko, G. A. & Sligar, S. G. (2000). *Science*, **287**, 1615–1622.
Schlichting, I., Jung, C. & Schulze, H. (1997). *FEBS Lett.* **415**, 253–257.
Sligar, S. G., Lipscomb, J. D., Debrunner, P. G. & Gunsalus, I. C. (1974). *Biochem. Biophys. Res. Commun.* **61**, 290–296.
Sundaramoorthy, M., Terner, J. & Poulos, T. L. (1995). *Structure*, **3**, 1367–1377.
Varadarajan, R., Zewert, T. E., Gray, H. B. & Boxer, S. G. (1989). *Science*, **243**, 69–72.
Watanabe, R., Usami, N. & Kobayashi, K. (1995). *Int. J. Radiat. Biol.* **68**, 113–120.
Weik, M., Berges, J., Raves, M. L., Gros, P., McSweeney, S., Silman, I., Sussman, J. L., Houee-Levin, C. & Ravelli, R. B. G. (2002). *J. Synchrotron Rad.* **9**, 342–346.
Weik, M., Ravelli, R. B. G., Kryger, G., McSweeney, S., Raves, M. L., Harel, M., Gros, P., Silman, I., Kroon, J. & Sussman, J. L. (2000). *Proc. Natl. Acad. Sci. USA*, **97**, 623–628.
Willard, J. E. (1973). *Science*, **180**, 553–561.
Wilmot, C. M., Sjogren, T., Carlsson, G. H., Berglund, G. I. & Hajdu, J. (2002). *Methods Enzymol.* **353**, 301–318.
Wuerges, J., Lee, J. W., Yim, Y. I., Yim, H. S., Kang, S. O. & Carugo, K. D. (2004). *Proc. Natl. Acad. Sci. USA*, **101**, 8569–8574.
Yano, J., Kern, J., Irrgang, K. D., Latimer, M. J., Bergmann, U., Glatzel, P., Pushkar, Y., Biesiadka, J., Loll, B., Sauer, K., Messinger, J., Zouni, A. & Yachandra, V. K. (2005). *Proc. Natl. Acad. Sci. USA*, **102**, 12047–12052.
Zaloga, G. & Sama, R. (1974). *Nature (London)*, **251**, 551–552.